Aging and Disease
www.aginganddisease.org
Volume 9, Number 2; 228-234, April 2018
http://dx.doi.org/10.14336/AD.2017.0415

Original Article

Brain Interstitial Fluid Drainage Alterations in Glioma-Bearing Rats

Xiangping Guan[1, 2], Wei Wang[1, 2], Aibo Wang[1, 2], Ze Teng[1, 2], Hongbin Han[1, 2,*]

[1]Department of Radiology, Peking University Third Hospital, Beijing 100191, China
[2]Beijing Key Lab of Magnetic Resonance Imaging Device and Technique, Beijing 100191, China

[Received March 9, 2017; Revised April 8, 2017; Accepted April 15, 2017]

ABSTRACT: Real time imaging and measurement of the drug distribution in the brain interstitial space (ISS) are able to determine the effeicency of local brain drug delivery to treatment gliomas. In the present study, we used a tracer-based magnetic resonance imaging (MRI) method to quantitatively analyze the effects of glioma growth on ISF drainage. Sprague-Dawley rats were randomly divided into six groups (n = 6). C6 glioma cells were implanted into either the caudate nucleus or thalamus of rats and then were examined 10 or 20 days after implantation. The two control groups were treated with vehicle. A tracer was injected into the caudate nucleus of control rats and rats with gliomas growing in the thalamus for 10 or 20 days. The tracer was similarly injected into the thalamus of control rats and rats implanted with gliomas in the caudate nucleus. The diffusion and clearance parameters of the tracer were calculated using tracer-based MRI techniques. We found that glioma implanted in the caudate nucleus significantly decreased the speed of the ISF flow in thalamus. With the growth of the glioma in thalamus, the drainage route of the brain ISF flow was altered in the caudate nucleus, but the speed of the flow was not significantly changed. These findings indicate that tracer-based MRI is a promising technique for optimizing the interstitial administration of therapeutics aimed at treating brain gliomas.

Key words: MRI, Gd-DTPA, glioma, interstitial fluid

Gliomas are the most common type of primary malignant tumor in the central nervous system. Patients with glioblastoma have poor prognosis, with a median survival of approximately 12–15 months [1, 2]. The efficacy of chemotherapy is currently limited by the blood–brain barrier, which precludes certain substances from entering the interstitial fluid (ISF). Yet the only approach that drugs can act upon nerve cells is to enter the ISF, since the latter is the microenvironment of nerve cells. Valuable findings had been recently reported that ISF plays a number of roles in brain function under physical and pathological conditions [3].

Direct drug delivery is one of several methods that may be used to circumvent this restriction, but limitations in the ability to monitor drugs distributed in the ISF system have prevent this technique from being reliable and reproducible. Moreover, the parameters required for direct local drug administration (e.g., delivery pressure, time, and frequency) are mostly acquired through experience [4].

A tracer-based magnetic resonance imaging (MRI) technique, which visualizes interstitial fluid drainage and measures parameters in the area of the glioma, can view the whole brain as well as ISF drainage in real time [5, 6]. The precise interstitial treatment of the glioma must be

***Correspondence should be addressed to:** Hongbin Han MD, Professor, Department of Radiology, Peking University Third Hospital, Beijing 100191, China. Email: hanhongbin@bjmu.edu.cn.

based on a full understanding of the interstitial fluid drainage changes in the brain. We are not only concerned about changes of interstitial fluid inside the tumor, but also concerned about the interstitial fluid drainage outside the tumor. In our previous studies, we have found that the interstitial fluid drainage in the tumor slows down due to tumor growth [7].

In this study, we used the tracer-based MRI to determine the effects of tumor growth on ISF drainage in deep brain regions by implanting C6 glioma cells into two regions of the rat brain and measuring changes in ISF drainage outside the tumors.

MATERIALS AND METHODS

Brain glioma model

All animal experiments were performed following the approval of the Ethics Committee of Peking University Health Science Center (Approval No. LA 2012-016).

Male Sprague–Dawley rats (weight, 250-300 g) were randomly divided into the following six groups (n=6). Group A: tracer injected into the caudate nucleus of normal rats; Group B: tracer injected into the thalamus of normal rats; Group C: tracer injected into the caudate nucleus after C6 cells had been implanted in the thalamus for 10 days; Group D: tracer injected into the caudate nucleus after C6 cells had been implanted in the thalamus for 20 days; Group E: tracer injected into the thalamus of rats with a glioma that had been grown in the caudate nucleus for 10 days; Group F: tracer injected into the thalamus of rats with a glioma that had been grown in caudate nucleus for 20 day.

Each experimental rat was anesthetized with intraperitoneal injection of pentobarbital sodium (50 mg/kg). To implant C-6 glioma cells, the rats' skin was incised and a small a hole (1.0 mm diameter) was drilled into the skull above the target implantation region: for the caudate nucleus, the coordinates were −0.8 mm, +2 mm, and 6 mm ventral; for the thalamus, +2.5 mm, +2.5 mm and 6.5 mm ventral. The C6 cells (10 μl, 1×10^5 cells) were injected into the brain with a Hamilton microsyringe at a rate of 1 μL/min.

Tumor detection

MRI examination was performed using a 3.0 T MRI scanner (Siemens, Germany). T2-weighted imaging (T2WI) sequence was used to detect the tumors at 10 and 20 days after implantation with the parameters as follows: repetition time, 3600 ms; echo time, 91 ms; flip angle, 120°; field of view, 80 mm; matrix, 256 × 256; slice thickness, 2 mm; three averages.

MR scan with tracer

Tracer scanning sequence was using a T1-weighted magnetization-prepared rapid acquisition with gradient-echo sequence (T1WI–MPRG): repetition time, 1500 ms; echo time, 3.7 ms; inversion time, 900 ms; flip angle, 9°; matrix, 512 × 96; field of view, 267 mm; voxel, 0.5 × 0.5 × 0.5 mm; two averages. A pre-scanning was performed to acquire a reference image and establish puncture positions for the caudate nucleus and thalamus.

Gd-DTPA (Magnevist, Bayer, Germany), diluted with double-distilled water to 10 mmol/L, was microinjected (2 μL, 0.2 L/min) into the caudate nucleus of rats in groups A, C, and D and into the thalamus of rats in groups B, E, and F. After the injection, the needle remained in place for 5 min before it was slowly extracted. A continuous T1WI-MPRG sequence was performed until the appearance of the images had nearly recovered to those acquired at T0.

Calculation of interstitial fluid flow parameters

The calculation of interstitial fluid flow parameters used in this study has been applied in: Transportation in the interstitial space of the brain can be regulated by neuronal excitation [8], the calculation is as below:

Substances in the extracellular space (ECS) follow the diffusion equation

$$\frac{\partial C}{\partial t} = D^* \cdot \nabla^2 C - \vec{v} \cdot \nabla C - \frac{f(C)}{\alpha} + \frac{Q}{\alpha}$$

where the diffusion coefficients of a given molecule in free media and brain ECS are D and D*, respectively, C is related with time and position, indicating the actual concentration in ECS, ∇^2 and ∇ represents the spatial derivatives in the appropriate coordinate system, v is the flow rate of the ISF in the ECS, f(C) denotes the clearance rate of probe in ECS, Q is the concentration of the diffusion source in ECS, and α is the volume fraction of the ECS within the brain. Because Gd-DTPA was not administered continuously, it was taken to be injected at the initial time point, and the value of Q was negligible in this study. The region of interest was as close as possible to the injection site (2 mm), and thus the quality of diffusion was assumed to have had no effect. It was also assumed that the ISF in the local ECS did not flow in a straight line. The following formula was used to calculate the diffusion parameters:

$$X = \sum_{i=1}^{n} \int_0^{r_0} \left(\Delta SI(r, t_i) - \Delta S\,\mathrm{I_m}(r, t_i) \right)^2 dr$$

Where $\Delta SI_m(r,ti)$ represents the radial range of diffusion measured at time *ti*. The diffusion parameters *D* and *k'* were measured using the time model and the measured curve. Tortuosity (λ) = $(D / D^*)^{1/2}$. The model's predicted profiles and measured profiles at a given time point were minimized to find the effective diffusion coefficient (D*), free diffusion coefficient (D), rate constant (k') and tortuosity (λ). The half time ($t_{1/2}$) was determined using linear fit.

The relationship between signal intensity and Gd-DTPA concentration (3.0-T MRI, T1WI–MPRG) has been reported previously (6).

Immunohistochemical analysis

After perfusion with 4% paraformaldehyde, brain tissues were removed and embedded in paraffin. Coronal sections were sliced to a thickness of 5 μm and then deparaffinized. Heat-mediated antigen retrieval was performed at pH 6.0. Sections were incubated overnight at 4°C with a primary antibody against tenascin C (rabbit anti-rat; 1:300; Abcam, Cambridge, UK), washed, and then incubated with a secondary antibody for 30 min at room temperature. The sections were stained with diaminobenzidine and counterstained with hematoxylin.

Data and statistical analyses

Image analysis was performed using Matlab imaging software (MathWorks, Natick, MA, USA). Tumor volumes were calculated by the equation $V \approx 4/3 \times \pi \times (0.5)^3 \times (abc)$, as a, b and c represent the length, width and height of the tumor, respectively. Statistical analyses were conducted using APSS 19.0 and Excel 2010 (Microsoft Co., Redmond, WA, USA). One-way analysis of variance was used to examine differences among multiple groups, and values of P less than 0.05 were considered to be significantly significant.

RESULTS

Glioma implanted in rat brain assessed with MRI

Tumor formation and growth were observed with T2-weighted imaging (T2WI) 10 and 20 days after the C6 glioma cells were implanted into either the thalamus or caudate nucleus of rats (Fig. 1). Significant increases in tumor volume were demonstrated in all implanted groups as shown in Figure 1.

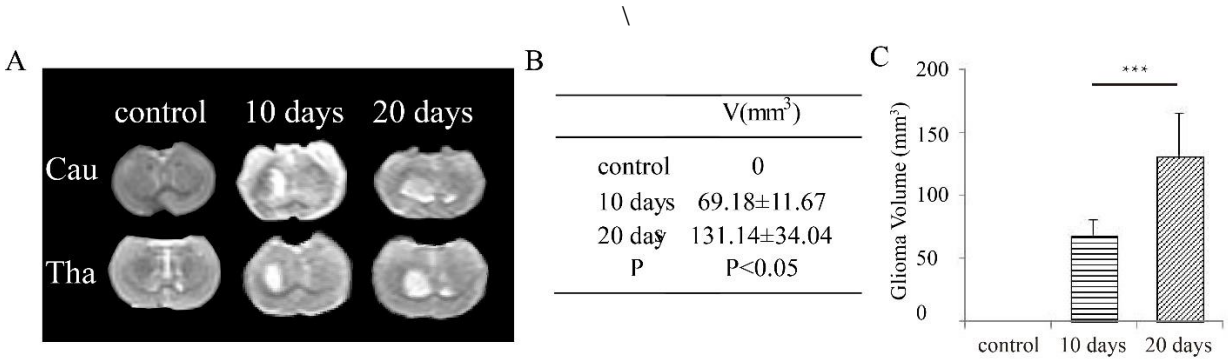

Figure 1. MRI images of gliomas in the caudate nucleus and thalamus of control groups and 10 and 20 days after implantation. Images acquired using T2WI of control groups and 10 and 20 days after implantation (**A**). Volume of the gliomas of control groups and 10 and 20 days after implantation (**B**). Tumor volume significantly increased from 10 to 20 days after implantation (**C**). ****P*<0.05.

ISF flow changes in the caudate nucleus after tumor implantation in the thalamus

Injection of Gd-DTPA into the caudate nucleus resulted in local MRI signal hyperintensities (Fig. 2 and 3). With the diffusion of Gd-DTPA into the ECS, the high-signal intensity region gradually expanded. Significant differences were demonstrated in the effective diffusion coefficient (D*), with D* increased in tumor groups: group C, $(6.91 \pm 4.24) \times 10^{-5}$ mm²/s; group D, $(10.39 \pm 8.33) \times 10^{-5}$ mm²/s); $P < 0.05$ compared with control group A, $(33.33 \pm 3.46) \times 10^{-5}$ mm²/s. Significant differences were also demonstrated in the clearance rate coefficient (k') between groups A and group D ($P < 0.05$), but not between groups A and C, or C and D: group A, $(0.65 \pm 1.00) \times 10^{-5}$ mm²/s; group C, $(2.00 \pm 2.36) \times 10^{-5}$

mm^2/s; group D, $(3.04 \pm 2.01) \times 10^{-5}$ mm^2/s. There were no differences in $t_{1/2}$ among the three groups: group A, 1.47 ± 0.21 h; group C, 1.24 ± 0.21 h; group D, 1.39 ± 0.21 h; $P > 0.05$. However, groups A, C, and D showed significantly different tortuosity values: group A, 1.32 ± 0.34; group C, 3.03 ± 0.91; group D, 2.65 ± 0.94; $P < 0.05$. We also observed pathway changes in the ISF flow among groups A, C, and D, which the magnetic tracer in group D reach the edge of cortex at the early stage of diffusion (Fig. 3), and the magnetic tracer in groups C hardly get into the cortex (Fig. 2B).

Because figure 2 and 3 share the same control group, the distribution pattern of Gd-DTPA in the control group have been included in figure 2 (Fig. 2A).

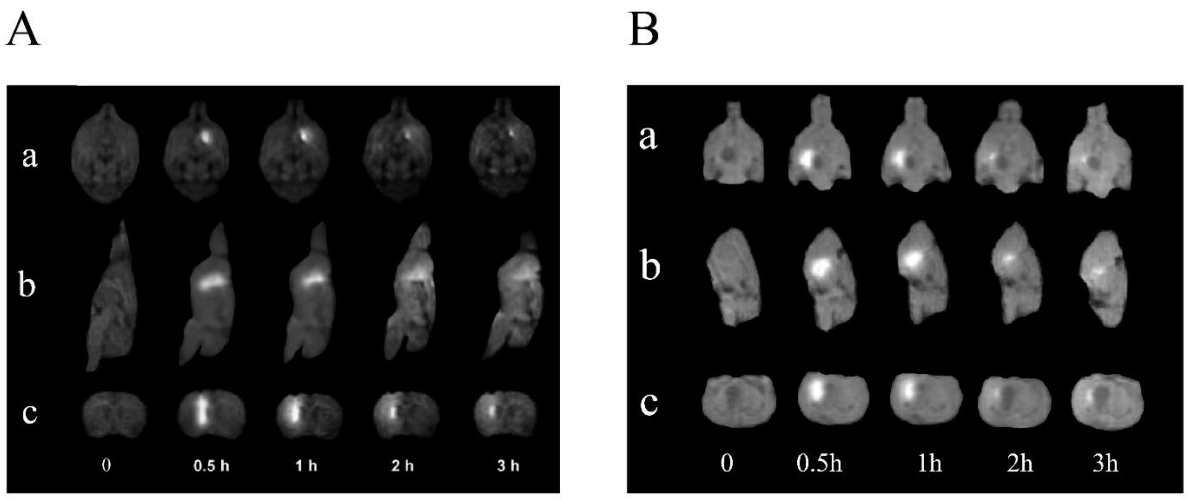

Figure 2. Gd-DTPA distribution in the caudate nucleus of control group and of the 10-day tumor (thalamus) group in axial plane (a), sagittal plane (b) and coronal plane (c). A) normal control group; **B**) the 10-day tumor (thalamus) group.

ISF flow alterations in the thalamus after tumor implantation in caudate nucleus

The MR images of the Gd-DTPA distribution in the thalamus of groups B, E and F are shown in Figure 4. With the diffusion of Gd-DTPA into the ECS, the high-signal intensity region gradually expanded but remained confined to the adjacent region. Significant differences were demonstrated in the effective diffusion coefficients (D*) among groups B, E, and F: group B, $(33.72 \pm 3.87) \times 10^{-5}$ mm^2/s; group E, $(17.33 \pm 11.27) \times 10^{-5}$ mm^2/s; group F, $(5.26 \pm 1.06) \times 10^{-5}$ mm^2/s; $P < 0.05$). Significant differences in the clearance rate coefficients (k') were also demonstrated, and the values for k' in the tumor groups (groups E and F) were increased compared with that in the normal group: group B, $(1.55 \pm 0.78) \times 10^{-5}$ mm^2/s; group E, $(2.80 \pm 2.60) \times 10^{-5}$ mm^2/s; group F, $(2.92 \pm 0.86) \times 10^{-5}$ mm^2/s; $p < 0.05$. We also found significant increases in t1/2 between the tumor groups (10 and 20 days after implantation) and the normal group (group B, 0.81 ± 0.03 h; group E, 1.47 ± 0.24 h; group F, 1.46 ± 0.55 h; $p < 0.05$) as well as significant increases in tortuosity (λ) in the tumor group 10 and 20 days after the implantation (group E, 2.76 ± 1.07; group F, 3.13 ± 0.33) compared with that in the normal group (group B, 1.23 ± 0.64; $p < 0.05$). However, pathway changes for the ISF flow in the thalamus were not observed after tumor implantation in the caudate nucleus, with alterations observed only in the stated parameters.

Immunohistochemical analysis of an extracellular matrix molecule in gliomas implanted in the thalamus for 10 and 20 days

Immunohistochemical analysis was performed to detect tenascin C changes in the extracellular matrix of gliomas implanted in the thalamus of the rat brain for 10 and 20 days. No accumulation was demonstrated in the ISS outsides the glioma, while, larger amounts of tenascin C accumulated in the extracellular matrix of the 20-day group (Fig. 5C) compared with the 10-day group (Fig. 5B).

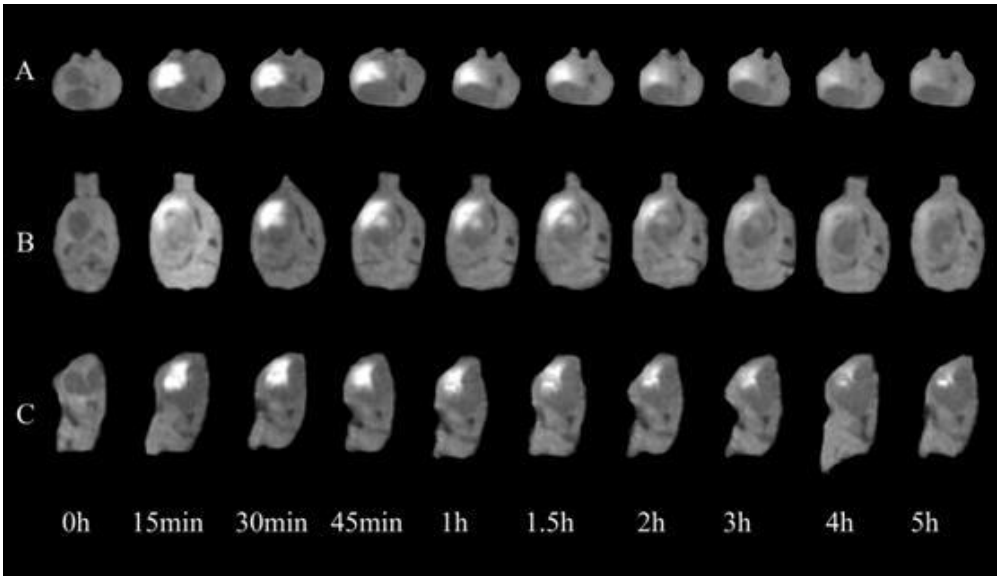

Figure 3. Gd-DTPA distribution in the caudate nucleus outside of the tumor (thalamus) in the 20-day group. **A**) axial plane; **B**) sagittal plane; **C**) coronal plane.

DISCUSSION

In the present study, we demonstrated that the ISF flow in regions adjacent to a glioma was altered with the growth of the tumor in the deep brain. Glioma in the caudate nucleus caused a significant decrease in the speed of the ISF flow in the thalamus. As the glioma grew in the thalamus, the drainage route for the ISF flow was altered in the caudate nucleus, but the speed of that flow was not significantly altered. We also found that the ISF flow did not transport molecules from the interstitial space (ISS) outside the glioma to the peripheral region of the glioma. The tracer distribution of ISF and flow bypassed the glioma, as it appeared as a high-intensity signal that wrapped around the glioma.

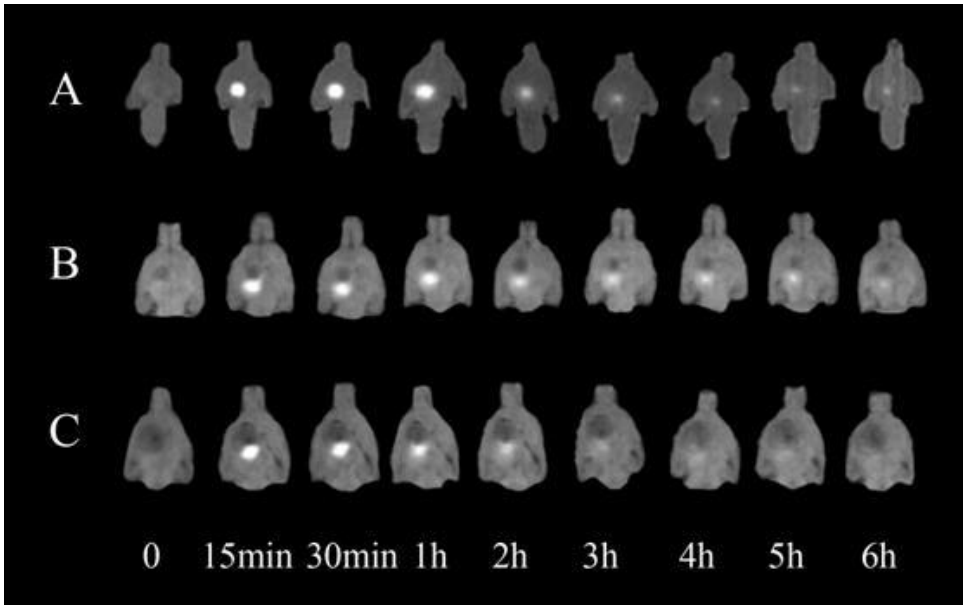

Figure 4. **Gd-DTPA distribution in thalamus in the axial plane. A**) normal control group; **B**) 10-day glioma in the caudate nucleus; **C**) 20-day glioma in the caudate nucleus.

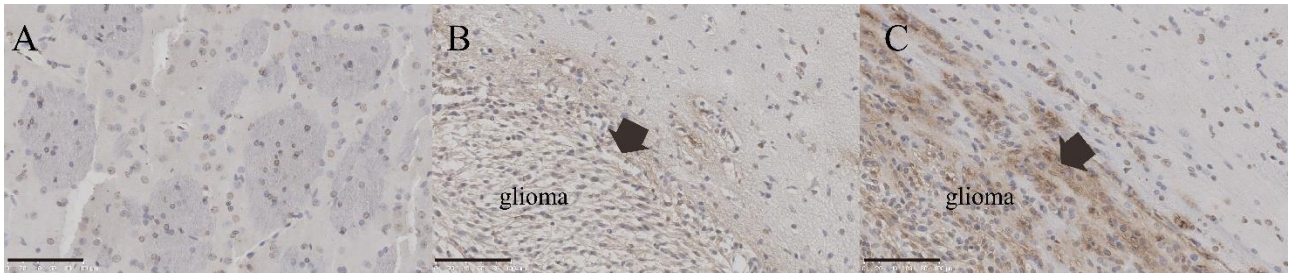

Figure 5. Thalamic Tenascin-C expression in control group and in the rats with glioma for 10-day and 20-day. Tenascin-C expression in thalamus of control group (**A**). Tenascin-C expression in thalamus of rats with glioma for 10-day (**B**). Tenascin-C expression in thalamus of rats with glioma for 20-day (**C**). Arrow identify the location of tenascin-C expression. Scale bar, 100 μm.

Early studies reported that some of the matrix components excessively expressed with tumor growth and caused the tortuosity of the brain ECS were increased inside the tumor [9, 10]. Our immunohistochemical results demonstrated that the expression of tenascin C increased with the growth of the glioma. The pressure inside the tumor is greater than that in the surrounding tissue, and the interstitial fluid inside the tumor flows from the centerline to the edge [11, 12]. In the present study, we found that diffusion in the brain ECS was strictly limited to inside the glioma [7, 13], and the diffusion in the brain ISS surrounding the tumor was similarly restricted, with significant changes in the ISF flow rate and flow route. This effect became more pronounced with increasing tumor volume. The different drainage route of the brain ISF in the caudate nucleus was demonstrated when the tumor was implanted in the thalamus. The drainage route was damaged at 10 days and presented as an inability of the ISF to drain into the cortex. At 20 days, the mass effect of the tumor squeezed and distorted the caudate nucleus; the ISF drainage route was demonstrated to be through narrow strips, and the brain ISF again drained to the parenchymal margin of cortex. However, we also found that the ISF flow is also related to the location of the tumor. In a previous study, we have showed that the interstitial spaces within the caudate nucleus and thalamus have different diffusion and flow parameters.

Although the mechanisms underpinning the regionalization of the ISF drainage in the deep brain will require further study, our results provided valuable insights for convection-enhanced delivery (CED) treatments of glioma. CED, which utilizes a convective pattern rather than simple diffusion, directs small molecules or macromolecules into the ISS, where they are distributed to the target [14]. Theoretically CED can maximize the brain concentration of the treatment drug with minimal systemic exposure and toxicity [15]. It has been found that the concentration of the drug injected into the brain by CED can reach more than a thousand times that following traditional drug administration, and the region in which the drug is applied can be relatively vast [16-19]. However, the use of CED has been limited in clinical practice because of the difficulty in monitoring and controlling the concentration and distribution of the injected drugs [20].

In summary, our results demonstrated that tracer-based MRI provides a real-time in vivo method for monitoring alterations in deep brain ISF drainage. Our findings also indicated that placement of CED administration should be designed based on the divisions of the brain ISS and should take into account potential changes in the brain ISS and ISF flow based on the location of the tumor as well as on the changes in the clearance rate and drainage pathways outside the tumor as the volume of the tumor grows. The tracer-based MRI will play a more and more important role in the optimizing the interstitial administration of therapeutics aimed at treating brain gliomas.

Acknowledgement

This work was supported by the National Natural Science Foundation of China (No. 81471633), the National Science Fund for Distinguished Young Scholars (No. 61625102) and the Beijing Municipal Science and Technology Commission (No. Z161100000116041).

References

[1] Stummer W, Pichlmeier U, Meinel T, Wiestler OD, Zanella F, Reulen HJ (2006). Fluorescence-guided surgery with 5-aminolevulinic acid for resection of malignant glioma: a randomised controlled multicentre phase III trial. Lancet Oncol, 7: 392-401.

[2] Teo M, Martin S, Owusu-Agyemang K, Nowicki S, Clark B, Mackinnon M, et al (2014). A survival analysis of GBM patients in the West of Scotland pre- and post-introduction of the Stupp regime. Br J Neurosurg, 28: 351-5.

[3] Lei Y, Han H, Yuan F, Javeed A, Zhao Y (2016). The brain interstitial system: Anatomy, modeling, in vivo measurement, and applications. Prog Neurobiol, in press.

[4] Wang W, Sivakumar W, Torres S, Jhaveri N, Vaikari VP, Gong A, et al (2015). Effects of convection-enhanced delivery of bevacizumab on survival of glioma-bearing animals. Neurosurg Focus, 38:E8.

[5] Xu F, Han H,, Zhang H, Pi J, Fu Y (2011). Quantification of Gd-DTPA concentration in neuroimaging using T-1 3D MP-RAGE sequence at 3.0 T. Magn Reson Imaging, 29:827-34.

[6] Han H, Li K, Yan J, Zhu K, Fu Y (2012). An in vivo study with an MRI tracer method reveals the biophysical properties of interstitial fluid in the rat brain. Sci China Life Sci, 55:782-7.

[7] Li K, Han H, Zhu K, Lee K, Liu B, Zhou F, et al (2013). Real-time magnetic resonance imaging visualization and quantitative assessment of diffusion in the cerebral extracellular space of C6 glioma-bearing rats. Neurosci Lett, 543:84-9.

[8] Shi C, Lei Y, Han H, Zuo L, Yan J, He Q, et al (2015). Transportation in the Interstitial Space of the Brain Can Be Regulated by Neuronal Excitation. Sci Rep. 2015, 5:17673.

[9] Day JM, Olin AI, Murdoch AD, Canfield A, Sasaki T, Timpl R, et al (2004). Alternative Splicing in the Aggrecan G3 Domain Influences Binding Interactions with Tenascin-C and Other Extracellular Matrix Proteins. J Biol Chem, 279:12511-8.

[10] Mouw JK, Ou G, Weaver VM (2014). Extracellular matrix assembly: a multiscale deconstruction. Nat Rev Mol Cell Biol, 15:771-85.

[11] Wu M, Frieboes HB, McDougall SR, Chaplain MAJ, Cristini V, Lowengrub J (2013). The effect of interstitial pressure on tumor growth: Coupling with the blood and lymphatic vascular systems. J Theor Biol, 320:131-51.

[12] DuFort CC, DelGiorno KE, Carlson MA, Osgood RJ, Zhao C, Huang Z, et al (2016). Interstitial Pressure in Pancreatic Ductal Adenocarcinoma Is Dominated by a Gel-Fluid Phase. Biophys J, 110:2106-19.

[13] Mahesparan R, Read TA, Lund-Johansen M, Skaftnesmo KO, Bjerkvig R, Engebraaten O (2003). Expression of extracellular matrix components in a highly infiltrative in vivo glioma model. Acta Neuropathol, 105:49-57.

[14] Bobo RH, Laske DW, Akbasak A, Morrison PF, Dedrick RL, Oldfield EH (1994). Convection-enhanced delivery of macromolecules in the brain. Proc Natl Acad Sci U S A, 91:2076-80.

[15] Lang FF, Bruner JM, Fuller GN, Aldape K, Prados MD, Chang S, et al (2003). Phase I trial of adenovirus-mediated p53 gene therapy for recurrent glioma: Biological and clinical results. J Clin Oncol, 21:2508-18.

[16] Wang W, Sivakumar W, Torres S, Jhaveri N, Vaikari VP, Gong A, et al (2015). Effects of convection-enhanced delivery of bevacizumab on survival of glioma-bearing animals. Neurosurg Focus, 38:E8.

[17] Cooper I, Last D, Guez D, Sharabi S, Elhaik Goldman S, Lubitz I, et al (2015). Combined local blood-brain barrier opening and systemic methotrexate for the treatment of brain tumors. J Cereb Blood Flow Metab, 35:967-76.

[18] Chen PY, Ozawa T, Drummond DC, Kalra A, Fitzgerald JB, Kirpotin DB, et al (2013). Comparing routes of delivery for nanoliposomal irinotecan shows superior anti-tumor activity of local administration in treating intracranial glioblastoma xenografts. Neuro Oncol, 15:189-97.

[19] Miyata S, Kawabata S, Hiramatsu R, Doi A, Ikeda N, Yamashita T, et al (2011). Computed tomography imaging of transferrin targeting liposomes encapsulating both boron and iodine contrast agents by convection-enhanced delivery to F98 rat glioma for boron neutron capture therapy. Neurosurgery, 68:1380-7.

[20] Torres LA, Coca MA, Batista JF, Casaco A, Lopez G, García I, et al (2008). Biodistribution and internal dosimetry of the 188Re-labelled humanized monoclonal antibody anti-epidemal growth factor receptor, nimotuzumab, in the locoregional treatment of malignant gliomas. Nucl Med Commun, 29:66-75.